HAL
open science

Nonlinear optical organic–inorganic crystals: synthesis, structural analysis and verification of harmonic generation in tri-(o -chloroanilinium nitrate)

Hamza Athmani, Christian Kijatkin, Rim Benali-Cherif, Sébastien Pillet, Dominik Schaniel, Mirco Imlau, Nourredine Benali-Cherif, El-Eulmi Bendeif

To cite this version:

Hamza Athmani, Christian Kijatkin, Rim Benali-Cherif, Sébastien Pillet, Dominik Schaniel, et al.. Nonlinear optical organic–inorganic crystals: synthesis, structural analysis and verification of harmonic generation in tri-(o -chloroanilinium nitrate). Acta Crystallographica Section A : Foundations and Advances [2014-..], 2019, 75 (1), pp.107-114. 10.1107/S2053273318014122 . hal-02319758

HAL Id: hal-02319758

https://hal.univ-lorraine.fr/hal-02319758

Submitted on 18 Oct 2019

HAL is a multi-disciplinary open access archive for the deposit and dissemination of scientific research documents, whether they are published or not. The documents may come from teaching and research institutions in France or abroad, or from public or private research centers.

L'archive ouverte pluridisciplinaire **HAL**, est destinée au dépôt et à la diffusion de documents scientifiques de niveau recherche, publiés ou non, émanant des établissements d'enseignement et de recherche français ou étrangers, des laboratoires publics ou privés.

Nonlinear optical organic-inorganic crystals: Synthesis, structural analysis, and verification of harmonic generation in tri-(o-Chloroanilinium Nitrate)

Hamza Athmani[a,b], Christian Kijatkin[c,e], Rim Benali-Cherif[a], Sébastien Pillet[b], Dominik Schaniel[b], Mirco Imlau[c,e], Nourredine Benali-Cherif[a,d] & El-Eulmi Bendeif[b*]

[a] Laboratoire des Structures, Propriétés et Interactions Interatomiques, Université Abbes Laghrour-Khenchela, 40000 Khenchela, Algeria,
[b] Université de Lorraine, CNRS, CRM^2, Nancy, France
[c] School of Physics, Osnabrück University, 49076 Osnabrück, Germany
[d] Ecole Nationale Polytechnique, département de Génie des Matériaux, 25000, Constantine, Algeria
[e] Research Center for Cellular Nanoanalytics, CellNanOs, Osnabrück University, 49076 Osnabrück, Germany
Correspondence e-mail: el-eulmi.bendeif@univ-lorraine.fr

Abstract

Structural and non-linear optical (NLO) properties of a new anilinium hybrid crystal of chemical formula [$(C_6H_7NCl^+, NO_3^-)_3$] have been investigated. The crystal structure was determined from single crystal X-ray diffraction measurements performed at a temperature of 100K and shows that the compound crystalizes in a noncentrosymmetric space group ($Pna2_1$). The structural analysis was coupled to the Hirshfeld surfaces analysis to evaluate the contribution of the different intermolecular interactions to the formation of supramolecular assemblies in the solid state that obey nonlinear optical features. This analysis reveals that the studied compound is characterized by a three-dimensional network of hydrogen bonds and the main contributions are provided by the O…H, C…H, H... H and Cl...H interactions, which alone represent ~ 85% of the total contributions to the Hirshfeld surfaces. It is noteworthy that the Halogen…H contributions are quite comparable to those of H…H contacts. The nonlinear optical properties were investigated by nonlinear diffuse femtosecond-pulse reflectometry and the obtained results were compared to those of the reference material $LiNbO_3$. The hybrid crystals exhibit notable second (SHG) and third (THG) harmonic generation that confirms its polarity generated by the different intermolecular interactions. These measurements also highlight that the THG signal of the new anilinium compound normalized to its SHG counterpart is more pronounced than for $LiNbO_3$.

1. Introduction

Organic-inorganic hybrid materials have been extensively investigated due to their remarkable versatile properties. Among others, anilinium derivatives have received considerable attention in recent years, due to their interesting applications as starting materials in multiple industrial and pharmaceutical processes **(**Below *et al*., 2004; Yunnikova *et al*., 2013). The anilinium halides are used as precursors in the synthesis of azo dyes, pigments, pesticides, insecticides, antioxidants and cosmetic products (Cao *et al*., 2010; Wang et al., 2010). The m-chloroaniline is for example used as a precursor for the production of the widely used antimicrobial and bactericide *Chlorohexidine* (Bayar *et al*., 2017). These compounds are also employed in the elaboration of optoelectronic devices in particular with a focus to non-linear optical (NLO) features. A pronounced NLO efficiency in these materials is correlated to the high polarizability of the π-conjugated molecules of the organic part and to the extended network of the intermolecular interactions between the organic cations and the inorganic anions, which promotes the charge transfer within the materials. On the other hand, these compounds are well investigated because of the ease of synthetic approaches, for their chemical and mechanical stability and their ability to crystallize in non-centrosymmetric structures appropriate for even order NLO applications. Although the development of anilinium derivatives systems continues to grow and being the main research topic of several research groups, a search in the Cambridge Structural Database CSD (ConQuest Version 1.22, 2018) (Allen, 2002) for crystal structures containing chloroanilinium molecules results in 37 hits with only seven compounds crystallizing in a non-centrosymmetric space groups. Based on our experience in the synthesis of anilinium derivatives hybrid compounds (Bendeif *et al.*, 2005; Boutobba *et al*., 2010; Dadda *et al*., 2012; Takouachet *et al*., 2016) we prepared a new Chloroanilinium nitrate compound: tri(o-Chloroanilinium Nitrate): [$(C_6H_7NCl^+, NO_3^-)_3$] named hereafter ***o-ClAN***. The combination of the organic anilinium with the inorganic planar NO_3^- anion is expected to yield enhanced NLO properties with respect to non-planar anions (Bouchouit *et al*., 2010) if crystallization in a non-centrosymmetric space group is achieved.

2. Experimental

2.1. Synthesis and crystallization

Crystals of tri(o-chloroanilinium nitrate): [$(C_6H_7NCl^+, NO_3^-)_3$] (**Fig. 1**) were obtained by adding nitric acid to an aqueous solution containing o-chloroaniline in a 1:1 stoichiometric ratio. After three weeks of slow evaporation at room temperature, small brown single crystals appeared. All chemicals (reagents and solvents) used for the synthesis were purchased from Sigma Aldrich, and used without further purification.

2.2. Single crystal X-ray measurements

The single crystal X-ray diffraction experiments were performed at 100 K on a SuperNova Dual Wavelength Microfocus diffractometer equipped with a 135 mm Atlas CCD detector, using Mo K_α radiation (λ= 0.71073 Å). To ensure high redundancies, the intensity data were accurately collected using ω oscillation scans of 1° per frame repeated at different φ positions. The radiation exposure time was 30 s per frame. The *CrysAlis* program suite (Rigaku Oxford Diffraction, 2017) was used for the unit cell determination, data reduction and analytical absorption corrections. The diffraction frames have been indexed and integrated yielding 117559 reflections up to a maximum resolution of $\sin\theta_{max}/\lambda$=0.864 $Å^{-1}$ and merged to 13028 unique reflections (R_{int} = 0.072) with a coverage of reciprocal space of more than 99.6%. The corresponding structure was solved in the space group *P*-1 by direct methods and successive Fourier difference syntheses and refined against F^2 by weighted full-matrix least-squares methods using the *SHELXL97* program (Sheldrick, 2008). All non-H atoms were refined anisotropically. All calculations were carried out using the *WinGX* software package (Farrugia, 1999).The crystallographic data, measurements and refinement details are summarized in **Table 1.**

2.3. Hirshfeld surfaces calculations

The Hirshfeld surface (*HS*) is a useful concept for describing the influence of molecular interactions by partitioning the total electron density in the crystal into molecular fragments where the electron distribution of a sum of spherical atoms for the molecule dominates the corresponding sum over the crystal (Hirshfeld, 1977; Spackman & Jayatilaka., 2009). Thus, the *HS* can be considered as the boundaries delimiting the space occupied by the molecular electron density from those of its neighboring molecules in a crystal. The size and shape of the *HS* also allow qualitative and quantitative investigations as well as the visualization of the different intermolecular interactions. The *HS* presented in this work were calculated with the program *Crystal Explorer (*Wolff *et al*., 2012) and are mapped using the normalized contact distance (d_{norm}), which is calculated using the following formula:

$$d_{norm}=\frac{d_i-r_i^{vdW}}{r_i^{vdW}}+\frac{d_e-r_e^{vdW}}{r_e^{vdW}}$$

where d_{norm} represent the sum of the distances of any surface point to the nearest external (d_e) and internal (d_i) atoms, normalized by the Van der Waals radii of the atoms . It is also worth

noting that *HS* maps are characterized by a red-blue-white color scheme: red regions represent closer contacts and negative d_{norm} value; blue regions represent longer contacts and positive d_{norm} value; and white regions correspond to interactions with bond lengths exactly equivalent to the Vander Waals separation and with a d_{norm} value of zero.

From the 3-D d_{norm} surface, we can obtain 2-D fingerprint plots, allowing easy attribution and quantitative analysis of the contribution of all intermolecular contacts at the same time. Thus, these 2D plots summarize the nature and type as well as the contributions of all intermolecular interactions.

Table 1: Crystallographic and refinement details for the structures of tri(o-chloroanilinium nitrate) salt.

	tri(o-chloroanilinium nitrate)
Crystal data	
Chemical formula	$(C_6H_7ClN^+.NO_3^-)_3$
M*r*	571.76
Crystal system, space group	Orthorhombic, *Pna2₁*
Temperature (K)	100
a, *b*, *c* (Å)	16.8015 (5), 6.5945 (2), 22.4243 (6)
V (Å3)	2484.56 (12)
Z	4
Radiation type	Mo Kα
μ (mm^{-1})	0.43
Crystal size (mm)	0.1x0.05x0.1
Data collection	
Diffractometer	Oxford Agilent-SuperNova
No. of measured, independent and observed with [I > 2σ(I)] reflections	117559, 13028, 9377
Rint	0.072
(sin θ/λ)max ($Å^{-1}$)	0.864
Refinement	
R[F2> 2σ(F2)], wR(F2), S	0.047, 0.099, 1.07
No. of reflection	13028
No. of parameters	409
No. of restraints	1
H-atom treatment	All H-atom coordinates parameters refined
Δρmax, Δρmin (e Å-3)	0.45, -0.38
Absolute structure	Flack x determined using 3510 quotients [(I+)-(I-)]/[(I+)+(I-)] (Parsons, Flack and Wagner, Acta Cryst. B69 (2013) 249-259).
Absolute structure parameter	−0.050(16)

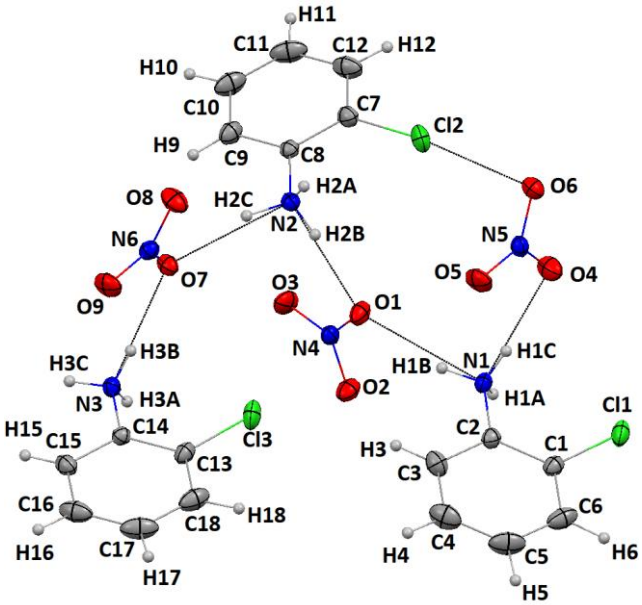

Figure 1. A view of the asymmetric unit ***o-ClAN*** with atom numbering scheme. Dashed lines indicate hydrogen bonds and halogen-oxygen interactions.

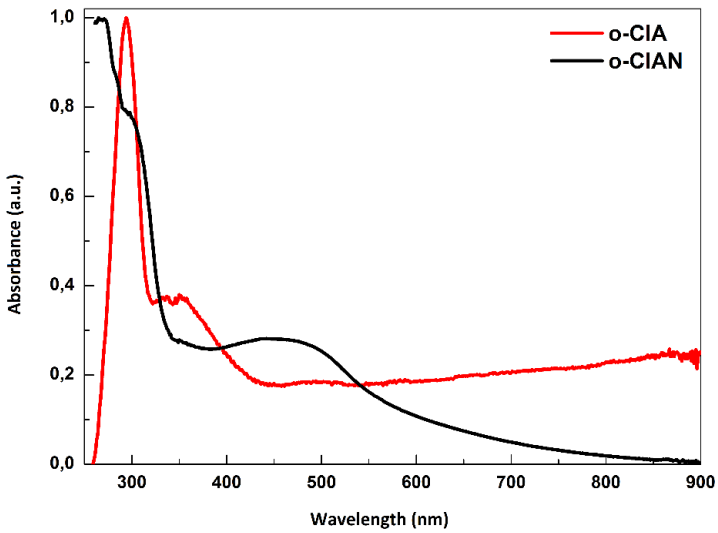

Figure 2. The absorption spectra of o-chloroaniline (***o-ClA)*** and ***o-ClAN*** *compounds***.**

2.4. UV-Visible spectra

The UV–Vis spectra of o-Chloroaniline and o-Chloroanilinium Nitrate ***(o-ClAN)*** samples are shown in **Figure 2**. The o-Chloroaniline compound has been measured for comparison. The measurements were performed in 10 mm quartz cell using a solution of low concentration (c $=10^{-5}$ mol/l) by dissolving the compounds in ethanol. The measurements were recorded at room temperature in the 250-900 nm range using a Cary 4000 Varian UV–Visible spectrophotometer. The spectra display mainly two absorption maxima at 293 nm and 350 nm for o-Chloroaniline and 269 nm and 450 nm for the hybrid compound (***o-ClAN***). The high energy absorption bands

are assigned to the π→π* transition and are attributed to the aromatic entities, while the lower energy absorption bands are assigned to the n→π* transition. We observe thus a clear red-shift of the low-energy band when forming the ***o-ClAN*** salt. .

2.5. Nonlinear optical measurement

Further structural information regarding the polarity of the sample were acquired through nonlinear diffuse reflectometry at room temperature. For more details, see reference (Kijatkin et al., 2017). For characterization, as-synthesized dry ***o-ClAN*** salt was compressed into a pellet for later irradiation. Using regeneratively amplified and spectrally tunable femtosecond pulses from a Ti:Sapphire laser system with a successive OPA (Astrella HE+, Coherent Inc. and TOPAS Prime, Light Conversion), light was slightly focused onto the sample surface. Incident peak intensities on the order of 10^{14} W/m^2 with a time-averaged power of 59 mW at λ = 1400 nm were applied for the generation of efficient second (SHG) and third harmonic emission (THG). Diffusely emitted light was collected at a small angle with a glass fiber and coupled into a spectrograph (IsoPlane SCT320 and PIXIS:2KB/BUV, Princeton Instruments). In order to compare absolute harmonic emission intensities, a second pellet was prepared from $LiNbO_3$:Mg nanopowder (henceforth abbreviated to **LNO, particle diameter approx. 70 nm**) whose nonlinear optical properties have been well-investigated and applied (Staedler *et al.*, 2012., Joulaud *et al*., 2013; Dutto *et al*., 2011; Rogov *et al*., 2015; Bonacina, 2013).

3- Results and discussion

3.1. Structure and crystal packing

The asymmetric unit of ***o-ClAN*** consists of three structurally independent o-chloroanilinium cations (***ClA-1:*** C1 to C6, ***ClA-2:*** C7 to C12 and ***ClA-3:*** C13 to C18) and three nitrate anions (N4-O1 to O3, N5-O4 to O6 and N6-O7 to O9) (**Fig. 1**). The organic cations and the nitrate anions are interconnected through hydrogen bonds and halogen-oxygen interactions (**Fig. 3**). This type of interactions has been observed in only one structure containing the o-chloroanilinium cation (Balamurugan *et al*., 2010) among the five structures deposited in the Cambridge Structural Database CSD (ConQuest Version 1.22, 2018) (Allen, 2002) . The crystal packing of ***o-ClAN*** is built of anionic zig-zag chains formed by the nitrate anions alternating with the o-chloroanilinium cations stacked layers parallel to the crystallographic ***c***-axis (**Fig. 4**). The three o-chloroanilinium cations are similar and show typical geometrical features to those observed in similar compounds (Bendeif *et al*., 2005; Boutobba *et al*., 2010; Dadda *et al*., 2012; Takouachet *et al*., 2016). The average C—N bond length for the o-chloroanilinium cations (1.456(2) Å) (**Table 2**) is longer compared to that observed for the o-chloroaniline compound (1.375(2) Å) (Nayak *et al*., 2009), indicating that the proton is transferred from the nitric acid to the amino group of the o-chloroaniline moieties. Compared to the o-chloroaniline structure (Nayak *et al*., 2009), the internal C—C—C angles at the halogen atoms decrease significantly [120.23(2)° vs 123.3(5)°] and the internal C—C—C angles at ammonium groups increase [120.39(13)° vs 115.6(5)°]. These angular changes are the consequences of the protonation of the amino groups (N1, N2 and N3) and of the implication of chlorine atoms in relatively short Cl···O halogen-oxygen interactions (Cl1···O7 = 3.087(2) Å and Cl2···O6 =

3.084(2) Å and Cl3…O1 = 3.288(2) Å). It is noteworthy that the three cations (***ClA-1***, ***ClA-2*** and ***ClA3***) form through their ammonium groups (N1, N2 and N3) four N—H⋯O hydrogen bonds with three different NO_3^- anionic neighbours (**Table 3**). Such intermolecular interactions produce ring motifs $R_3^5(16)$ between the organic cations and the nitrate anions **(Fig. 4)**.

Table 2 selected geometric parameters (Å, °)

Cl1—C1	1.733(2)	N4—O1	1.278(2)
Cl2—C7	1.731(2)	N4—O2	1.248(2)
Cl3—C13	1.729(2)	N4—O3	1.227(2)
N1—C2	1.453(2)	N5—O4	1.261(2)
N2—C8	1.459(2)	N5—O5	1.231(2)
N3—C14	1.458(2)	N5—O6	1.263(2)
C1—C2	1.387(3)	N6—O7	1.276(2)
C2—C3	1.390(3)	N6—O8	1.250(2)
C3—C4	1.388(3)	N6—O9	1.230(2)
C4—C5	1.374(5)	C12—C7	1.390(3)
C5—C6	1.392(4)	C13—C14	1.385(3)
C1—C6	1.389(3)	C14—C15	1.388(3)
C7—C8	1.386(3)	C15—C16	1.391(3)
C8—C9	1.387(3)	C16—C17	1.382(5)
C9—C10	1.390(3)	C17—C18	1.386(4)
C10—C11	1.385(4)	C18—C13	1.390(3)
C11—C12	1.387(4)	C1—C2—N1	119.72(18)
C2—C1—Cl1	119.01(16)	C3—C2—N1	120.17(18)
C6—C1—Cl1	120.45(17)	C7—C8—N2	119.77(17)
C8—C7—Cl2	119.20(15)	C9—C8—N2	119.81(18)
C12—C7—Cl2	120.65(18)	C13—C14—N3	119.79(17)
C14—C13—Cl3	119.43(15)	C15—C14—N3	119.60(18)
C18—C13—Cl3	120.56(17)		

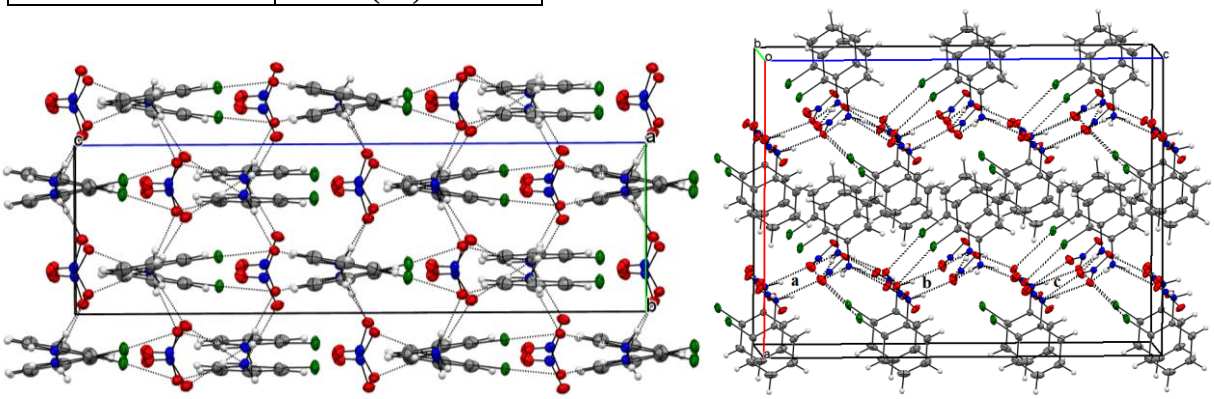

(a) **(b)**

Figure 3. Projection of the ***o-ClAN*** structure along: **(a)** the crystallographic ***a***-axis and **(b)** the **b** direction showing a periodic arrangement of anionic zig-zag chains formed by the nitrate anions and o-chloroanilinium cationic layers. Dashed lines indicate intermolecular interactions.

The geometrical features of the three nitrate entities show a distorted sp2 configuration. The O—N—O angles are relatively similar ranging from 117.41(16)° to 122.24(16)°. Each NO_3^- anion is characterized by one shorter N—O bond length and two longer ones (**see Table 2 for more details**). These significant differences in N—O distances [ranging from 1.227(2) Å to 1.278(2) Å] can be explained by the fact that the longest N—O bond lengths (**Table 2**) correspond to oxygen atoms involved in hydrogen bonds, however the shortest ones (N4—O3, N5—O5 and N6) correspond to those not implicated in any intermolecular interactions with organic cations. This behavior was also reported in a 4-nitroanilinium nitrate structure (Perpétuo *et al*., 2004).

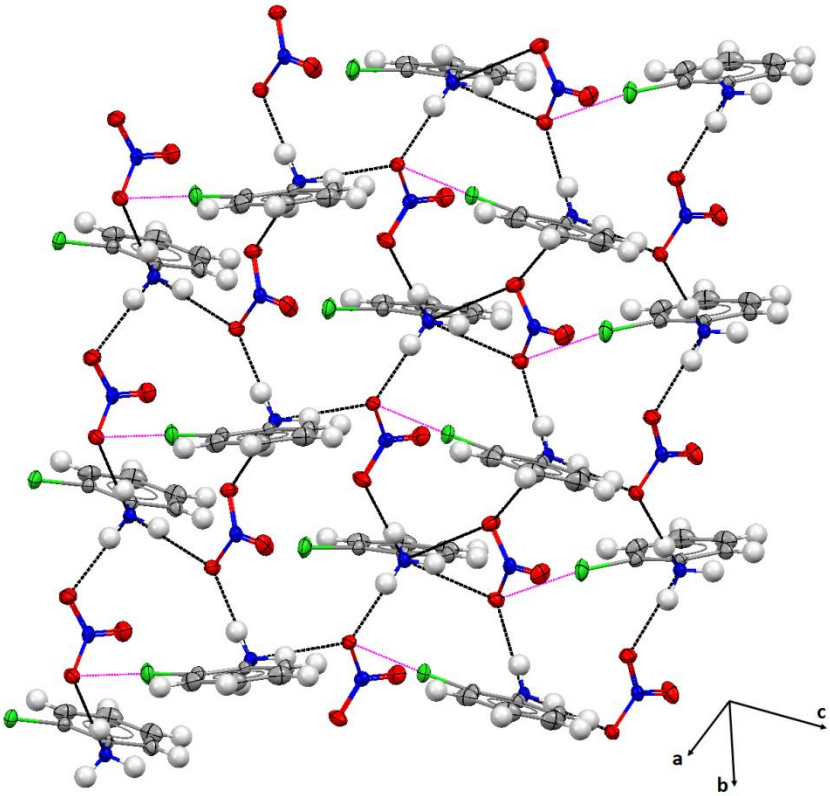

Figure 4. 3D view of the crystal packing of ***o-ClAN***, illustrating the formation of ring motifs $R_3^5(16)$ between organic cations and NO_3^- anions. N—H···O hydrogen bonds are represented by black dashed line and Cl···O interactions are illustrated by magenta dashed line.

3.2. Molecular Hirshfeld surfaces

The Hirshfeld surfaces of compound ***o-ClAN*** were mapped over d_{norm} (0.5 to 1.5 Å) and are illustrated in Figure 5. The red circular depressions visible in the front and back surface views indicate hydrogen bonding contacts (**Fig. 5**). The strongest and shortest interactions between N—H (N1—H1A, N2—H2A, N3—H3A and N3—H3C) and O (O2, O6 and O8) atoms manifest in the Hirshfeld surfaces as the eight (08) bright red areas. The other visible spots on the surfaces correspond to weak C—H···O and C—H···Cl hydrogen bonds.

Table 3: Hydrogen-bonding geometry (Å,°)

D—H···*A*	*D*—H (Å)	H···*A* (Å)	*D*···*A* (Å)	*D*—H···*A* (°)
N1—H1C···O4	0.82(3)	1.98(3)	2.800(2)	173(3)
N1—H1A···O6^{i}	0.85(3)	1.99(3)	2.825(2)	169(3)
N1—H1B···O1	0.89(3)	1.99(3)	2.858(2)	166(3)
N1—H1B···O2	0.89(3)	2.43(3)	3.095(2)	132(2)
N2—H2B···O1	0.87(3)	1.93(3)	2.799(2)	174(3)
N2—H2A···O2^{iv}	0.88(3)	1.96(3)	2.821(2)	166(3)
N2—H2C···O7	0.94(3)	1.90(3)	2.823(2)	166(2)
N2—H2C···O8	0.94(3)	2.53(3)	3.185(2)	127(2)
N3—H3B···O7	0.84(3)	1.95(3)	2.793(2)	175(2)
N3—H3A···O8^{i}	0.87(2)	1.96(3)	2.819(2)	171(3)
N3—H3C···O6^{ii}	0.87(4)	2.08(3)	2.904(2)	159(2)
N3—H3C···O4^{ii}	0.87(4)	2.34(3)	3.038(2)	138(2)

Symmetry code(s): (i) *x*, *y*-1, *z*; (ii) -*x*+1/2, *y*-1/2, *z*+1/2; (iii) *x*, *y*+1, *z*; (iv) *x*-1/2, -*y*+3/2, *z*.

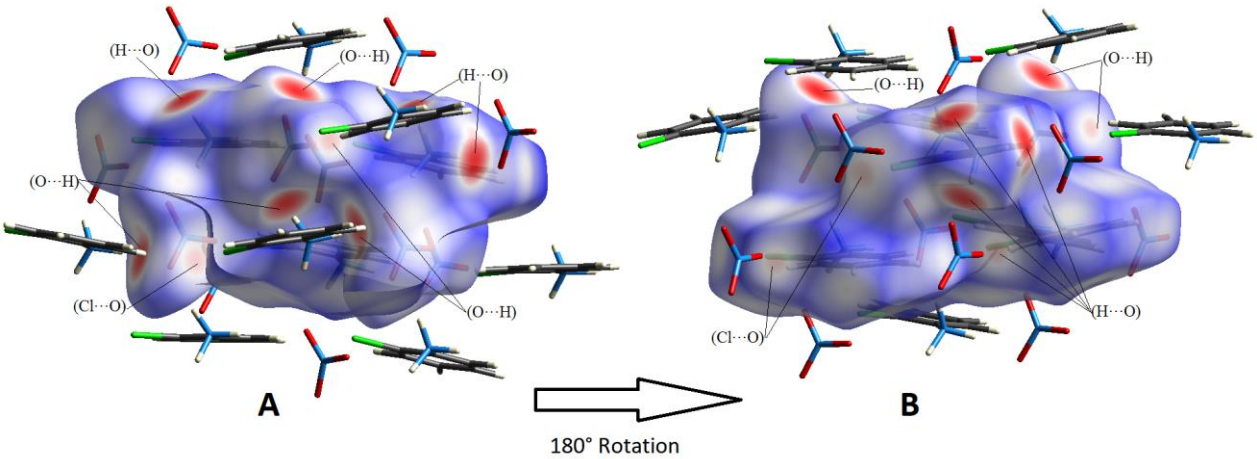

Figure 5. 3D Hirshfeld maps with d_{norm} in the range 0.5 to 1.5 Å: **A**: front view and **B** back view. Red circle indicating short hydrogen bonds.

The 2D fingerprint plots are used for identification and separation of intermolecular interactions and relative contribution of these interactions can be obtained from the area of the surfaces. The 2D fingerprint plots of the studied compound are shown in **Fig. 6**.

The O…H/H…O contacts, which are attributed to N—H…O hydrogen-bonding interactions, appear as two sharp symmetric spikes in the two dimensional fingerprint maps (**Fig. 6b**). They have the most significant contribution to the total Hirshfeld surfaces, accounting for more than

40.9%. The presence of these long spikes is characteristic of strong and short hydrogen bonds associated with the cation-anion interactions (**Table 3**). Moreover, significant contributions to the surfaces are made by the H…C/C…H contacts that appear as symmetrical wings (**Fig. 6c**) in the fingerprint plots and have a contribution of 19% of the total *HS*. The H…H contacts appear in the middle of the scattered points in the two-dimensional fingerprint maps (**Fig. 6d**). They were found to be the third highest contributors towards the Hirshfeld surface, after the H…O/O…H and H…C/C…H contacts, covering 13.9%. It is important to note that this analysis reveals a significant contribution of H...Halogen interactions (10.9%) comparable to that of H…H contacts. The H…Halogen interactions appear as wings on the top left (H…Cl) and bottom right (Cl...H) of the 2D fingerprint plots (**Fig. 6e**). Apart from the above interactions, the other interactions (Cl…C/C…Cl, O…O, Cl…O/O…Cl, N…H/H…N and C…C) are also observed and are highlighted in **Fig. 6f–j**. Their contributions are less than 5% of the total area of the *HS*.

From this analysis, we observe that the major contributions come from the four molecular interactions mentioned above, namely: the O…H/H…O, H…C/C…H, H...H and Cl... H/H…Cl. These interactions represent ~ 85% of the total contributions to the Hirshfeld surfaces and show the diversity of the intermolecular interactions leading to unusual nonlinear optical properties of this molecular compound. It has been also shown that the efficiency of the hydrogen-bond interactions play a key role in the significant enhancement of NLO properties compared to similar compounds ((Bouchouit *et al*., 2010; Sajana *et al*., 2010; Tanak *et al*., 2014).

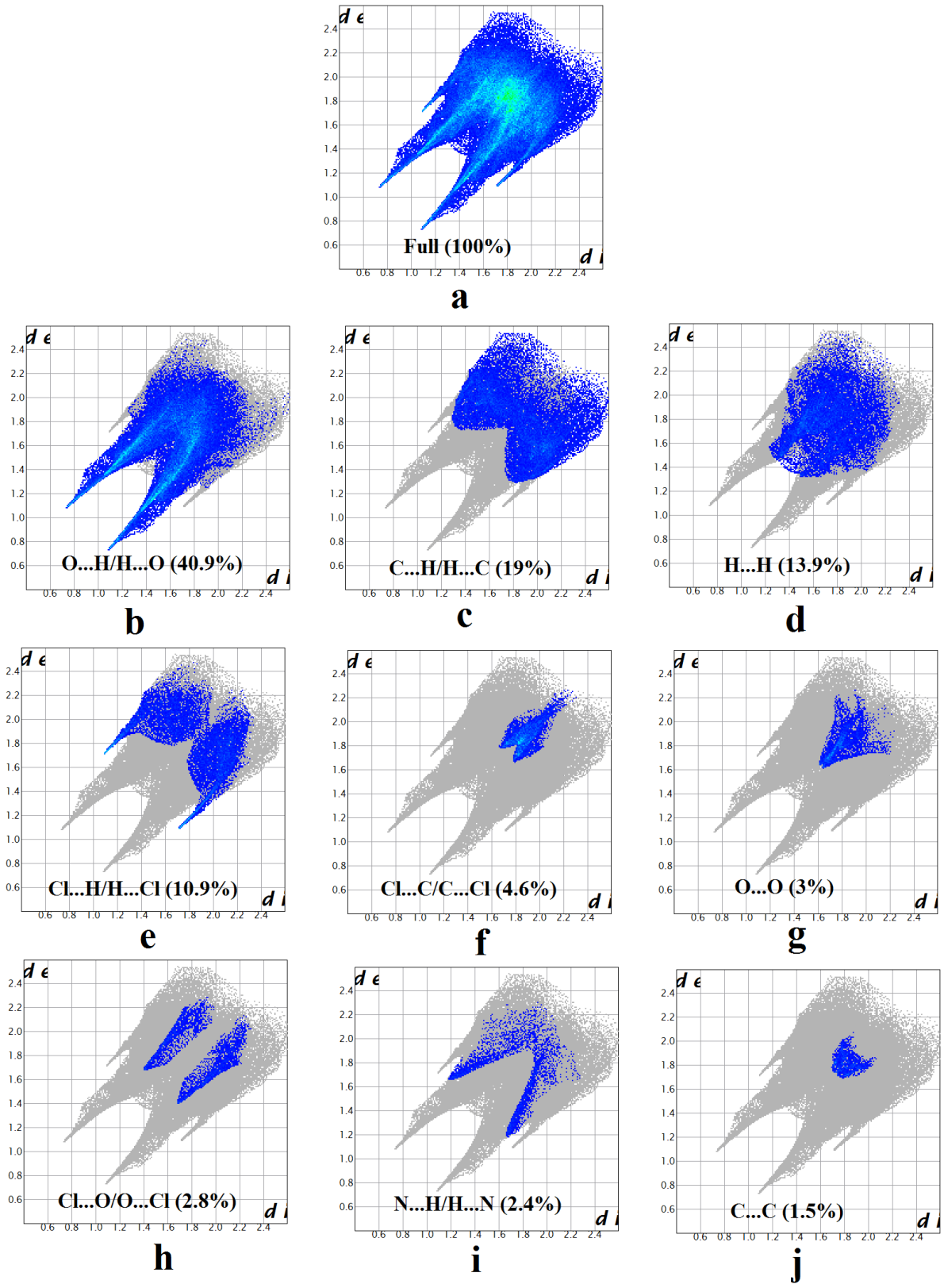

Figure 6. 2D fingerprint plots of ***o-ClAN*** compound for different intermolecular interactions.

3.3. NLO properties

Upon irradiation with femtosecond pulses (Incident peak intensities on the order of 1014 W/m^2 with a time-averaged power of 59 mW at λ = 1400 nm), ***o-ClAN*** hybrid crystal exhibit notable second and third harmonic generation at wavelengths of 700 nm and 467 nm, respectively. This is underlined by the measured harmonic ratio f_R (**see reference** (Kijatkin *et al*., 2017) **for the definition of f_R**) ranging up to 5.6×10^7 which approaches that of LNO being 1.0×10^9. This finding has two consequences: 1) because f_R is well above unity, this measurement confirms the polarity of the ***o-ClAN*** compound (Kijatkin *et al*., 2017), generated by the different intermolecular interactions discussed above and 2) the THG signal of ***o-ClAN*** normalized to its SHG counterpart is more pronounced than for LNO. Visual inspection confirms this finding: whereas LNO irradiated with a wavelength λ = 1400 nm appears in a red-magenta hue, ***o-ClAN*** incorporates relatively larger cyan components at 467 nm, thereby appearing in more blue hue. However, the nonlinear optical signal of the ***o-ClAN*** compound is highly time-dependent and deteriorates significantly upon prolonged exposure (**Fig. 7**).

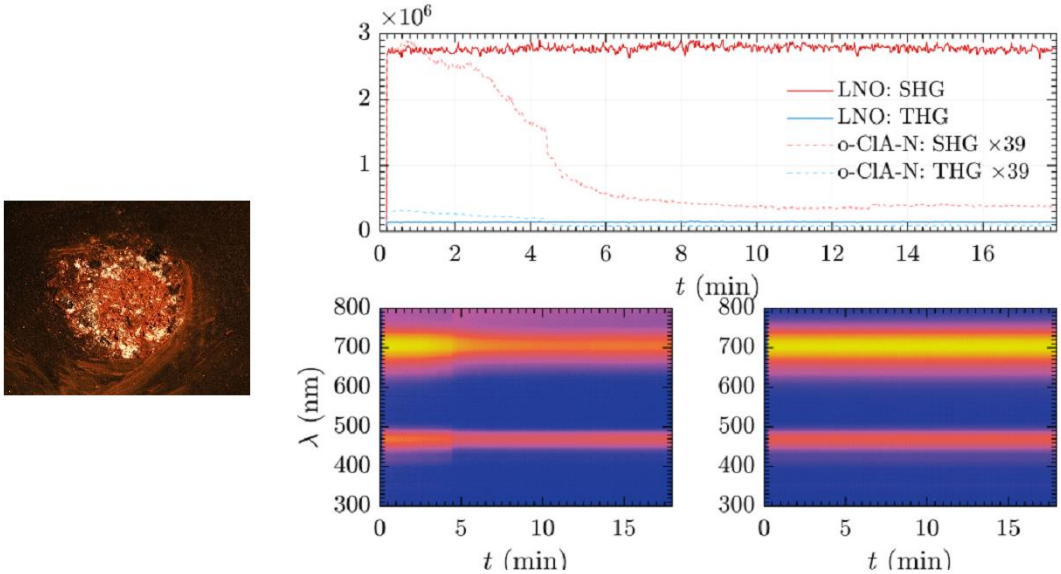

Figure 7. Left: ***o-ClAN***-pellet before exposure. The pellet measures 5 mm in diameter. **Right top:** second (red) and third (blue) harmonic emission from LNO (solid lines) and ***o-ClAN*** (dashed lines) as a function of time. SHG and THG signal of ***o-ClAN*** have been scaled for better visibility. **Right bottom:** normalized spectral traces for ***o-ClAN*** (left) and LNO (right) scaling from yellow (high) to blue (low signal).

During exposure, thermal damage of ***o-ClAN*** was observed at the irradiated spot which is the like cause for the time-dependent decline of harmonic signals. In contrast, LNO showed neither signal nor sample degradation over time. Moving the excitation spot on the ***o-ClAN***-pellet surface showed significant fluctuations in the overall emitted nonlinear signal. This can be related to the inhomogeneous surface of the ***o-ClAN***-sample (**Fig. 7**, **left**) which is only selectively illuminated.

Additional measurements at different positions on the sample revealed that the ***o-ClAN*** compound can occasionally challenge harmonic emission of polar materials for short timescales. In terms of the emitted SHG-signal at an incident wavelength λ = 1400 nm, ***o-ClAN*** typically ranges between 1/10 and 1/300 of the conversion efficiency of the LNO-nanocrystalline powder sample.

4. Conclusion

In summary, we have reported in this work the synthesis, structural characterization and nonlinear optical (NLO) properties of anilinium organic-inorganic crystal of formula [$(C_6H_7NCl^+, NO_3)_3$] (***o-ClAN***). The elaboration of this material was driven by the association of two molecular entities characterized by an electronic configuration favorable to charge transfer allowing therefore high polarizability expected to yield enhanced NLO properties.
The accurate structural analysis performed at low temperature (100K) shows that the crystal structure can be described in the pyroelectric crystalline symmetry class. The *Hirshfeld* surfaces analysis coupled to the structural investigation reveal that crystal packing is characterized by a three-dimensional network of hydrogen bonds and the main contributions are provided by the O…H, C…H, H... H and Cl...H interactions, which alone represent ~ 85% of the total contributions to the *Hirshfeld* surfaces. The different intermolecular interactions acting in accordance with the significant and directional H…H and H…Halogen contacts are responsible for steering molecules in the non-centrosymmetric space group leading to interesting NLO properties. The NLO measurements shows that the ***o-ClAN*** exhibits remarkable second (SHG) and third (THG) harmonic generation that confirms its polarity driven by the different intermolecular interactions. The obtained results were also compared to those of the reference material $LiNbO_3$ and show that THG to SHG ratio of the studied compound is more pronounced than for $LiNbO_3$.

Acknowledgements

This work was supported by the Université de Lorraine, the CNRS and PHC PROCOPE 40539XA, which are gratefully acknowledged. H.A. is indebted to the Algerian Ministry of Research and Université Abbes Laghrour-Khenchela for a doctoral fellowship. The authors would like to thank the Deutsche Forschungsgemeinschaft (DFG INST 190/165-1 FUGG) and German Academic Exchange Service (DAAD 57139940) for financial support. The authors like to thank Laura Oláh and Zsuzsanna Szaller from the Wigner Research Center for Physics, Budapest, for the preparation of LNO nanopowders within the project MÖB 65056 of the Hungarian Tempus Foundation.

References

Allen, F.H. (2002). *Acta Crystallogr*. **B58**, 380-388.

Balamurugan, P., Jagan, R. & Sivakumar, K., (2010). *Acta Crystallogr*. **C66**, o109-o113.

Bayar, I., Khedhiri, L., Jeanneau, E., Lefebvre, F & Ben Nasr, C. (2017). *Journal of Molecular Structure*. **1137**, 373-379.

Below, H., Lehan, N & Kramer, A. (2004). *Microchim, Acta* .**146**. 129–135.

Bendeif, E.-E., Dahaoui, S., François, M., Benali-Cherif, N & Lecomte, C. (2005). *Acta Crystallogr*. **B61**, 700-709.

Bonacina, L. (2013). *Mol. Pharmaceutics*. ***10*(3)**, 783–792

Bouchouit, K., Bendeif, E.-E., EL Ouazzani, H., Dahaoui, S., Lecomte, C., Benali-Cherif, N & Sahraoui, B. (2010). *Chemical Physics*. **375**, 1–7.

Boutobba, Z., Direm, A & Benali-Cherif, N. (2010). *Acta Crystallogr*. **E66**, o595-o596.

Cao, L; Z. Liu, T. Wang, H. Dai, L. Zhang, X. Tao & D. Cui. (2012). *CrystEngComm*. **14**, 5795–5800.

Dadda, N., Nassour, A., Guillot, B., Benali-Cherif, N & Jelsch, C. (2012). *Acta Crystallogr*. **A68,** 452-463.

Dutto, F., Raillon, C., Schenk, K. & Radenovic, A. (2011). *Nano Letters*. **11(6)**, 2517-2521

Farrugia, L. J. (1999). *J. Appl. Crystallogr*. **32,** 837-838.

Hirshfeld, E. L. (1977). *Theor. Chim. Acta*. 44, 129–138

Joulaud, C., Mugnier, Y., Gnon Djanta, Y., Dubled, M., Marty, J-C., Galez, C., Wolf, -P., Bonacina, L & Le Dantec, R. (2013). *Journal of Nanobiotechnology*. **11(Suppl 1**):S8.1-9.

Kijatkin, C., Eggert, J., Bock, S., Berben, D., Oláh, L., Szaller, Z., Kis, Z. & Imlau, M. (2017). *Photonics*. **4**, 11-24.

Nayak, S. K., Prathapa, S. J. & Row, T.N.G., (2009). *Journal of Molecular Structure*. **935**, 156-160.

Perpétuo, G. J & Janczak, J. (2004). *Acta Crystallogr*. **C60**, o768-o770.

Rigaku Oxford Diffraction. (2017) *CrysAlis CCD* and *CrysAlis RED* (*Versions 1.171.38.46*), Rigaku Oxford Diffraction. Yarnton, England

Rogov, A., Mugnier, Y & Bonacina, L., (2015). *J. Opt*. ***17***, 033001- 033012

Sajana, D., Ravindra, H.J., Neeraj Misra & Hubert Joe, I. (2010). *Vibrational Spectroscopy*. **54**, 72–80.

Sheldrick, G. M. (2008). *Acta Cryst*. **A64**, 112–122.

Spackman, M. A & Jayatilaka, D. (2009). *CrystEngComm*. **11**, 19-32.

Staedler, D., Magouroux, T., Hadji, R., Joulaud, C., Extermann, J., Schwung, S., Passemard, S., Kasparian, C., Clarke, G., Gerrmann, M., Le Dantec, R., Mugnier, Y., Rytz, D., Ciepielewski, D., Galez, C., Gerber-Lemaire, S., Juillerat-Jeanneret, L., Bonacina, L & Wolf, J-P. (2012). *ACS Nano*. ***6*(3)**, 2542-2549.

Takouachet, R., Benali-Cherif, R., Bendeif, E.-E., Benali-Cherif, N., Pillet, S & Schaniel, D. (2016). *Inorganica Chimica Acta*. **446,** 6–12.

Tanak, H., Pawlus, K., Marchewka, M.K & Pietraszko, A. (2014). *Spectrochimica Acta Part A: Molecular and Biomolecular Spectroscopy*. **118**, 82-93.

Wang, J. J., Wang, Y. Q., Cao, F. F., Guo, Y. G & Wan, L. J. (2010). *J. Am. Chem. Soc*. **132**, 12218–12221.

Wolff, S. K., Grimwood, D. J., McKinnon, J. J., Turner, M. J., Jayatilaka, D. & Spackman, M. A. (2012). *CrystalExplorer, Version 3.1. Perth*: University of Western Australia.

Yunnikova, L. P., Akent'eva, T. A & Aleksandrova, G. A. (2013). *Pharm. Chem. J*. **46**, 27–29.